Navigated range expansion promotes migratory culling

Yi Zhang[1], Qingjuan Hu[1], Yingtong Su[1], Pan Chu[1,2], Ting Wei[1], Caiyun He[1], Peilei Yu[1], Chenli Liu[1,2], Xiongfei Fu[1,2*]

[1]Key Laboratory for Quantitative Synthetic Biology, Shenzhen Institute of Synthetic Biology, Shenzhen Institutes of Advanced Technology, Chinese Academy of Sciences, Shenzhen 518055, China

[2]University of Chinese Academy of Sciences, Beijing 100049, China

*Corresponding author. Email: xiongfei.fu@siat.ac.cn

SUMMARY

Motile organisms can expand into new territories and increase their fitness[1–6], while nonmotile viruses usually depend on host migration to spread across long distances[7–9]. In general, faster host motility facilitates virus transmission[10]. However, recent ecological studies have also shown that animal host migration can reduce viral prevalence by removing infected individuals from the migratory group[11]. Here, we use a bacteria-bacteriophage co-propagation system to investigate how host motility affects viral spread during range expansion. We find that phage spread during chemotaxis-driven navigated range expansion decreases as bacterial migration speed increases. Theoretical and experimental analyses show that the navigated migration leads to a spatial sorting of infected and uninfected host in the co-propagating front of bacteria-bacteriophage, with implications for the number of cells left behind. The preferential loss of infected cells in the chemotactic front inhibits viral spread. Further increase in host migration speed leads to a phase transition that eliminates the phage completely. These results illustrate that navigated range expansion of host can promote the migratory culling of infectious diseases in the migration group.

Main

Range expansion is a process by which living species invade new territories and gain benefits such as survival, reproduction, and resources[12–14]. Classic theory predicts that motile populations expand in space and time by growing and moving[15–17]. Recent studies have shown that many organisms can use self-generated cues, known as navigated range expansion, to increase the expansion rate towards long-term settlement[18–22]. However, nonmotile species, have to use other strategies to expand their territories, such as viruses, which depend on the infected hosts to spread across long distances[7]. It is commonly assumed that host motility enhances virus transmission and viral range expansion[10,23–26]. However, recent ecological studies have also reported that animal host migrations can reduce viral prevalence[11,27–33]. This can occur when animals escape from infected regions ('migratory escape')[28,30] or when infected animals are removed from migrating populations ('migratory culling')[11,34]. One of prominent examples is that seasonal migration of butterfly monarchs reduces the risk of infection of parasites[11,27]. These conflicting findings from epidemiological case studies suggest that the effects of host spatial expansion on viral prevalence depend on the specific conditions of the system, which require a close and quantitative examination. However, studying infectious disease dynamics and their mechanisms in field studies is difficult due to the limitations of observatory technology and the complexity of the natural system. Therefore, we developed a co-propagation system with motile bacteria, *Escherichia coli* (*E.coli*), and its temperate bacteriophage M13, to investigate how host range expansion affect the

relationship between host motility and viral spatial prevalence.

Phage spread during the bacterial range expansion

We adopted a swimming assay of motile bacteria by inoculating a small droplet of cells at the center of a semi-solid agar plate (green dot in Fig. 1A, 2ul containing about 10^6 cells). The motile bacterial population grew and expanded radially. Ahead of the expanding bacterial population, we plated a small volume of nonlethal phage M13 (lightpink dot in **Figure 1a,** containing about 5×10^6 phage particles). When the bacteria encountered the phage zone, they became infected and temporarily reduced their growth (**Extended Data Figure 1**), resulting in a visible low-density region of infected zone compared to the uninfected zones (See SI Method, **Extended Data Figure 2**). To better identify the infected region, we integrated a red fluorescent gene *Ruby* into the M13 phage genome (**Extended Data Figure 3a**). The infection of M13 phage introduced the fluorescent gene into the bacterial cells, which expressed the red fluorescent protein (**Extended Data Figure 3a**). Therefore, the infected region can be detected by the fluorescent signal measurement, which coincides with the visible low-density region (**Figure 1b**, **Extended Data Figure 3b**).

To understand the dynamics of bacteria-phage co-propagation, we extended a growth-expansion model that incorporates bacterial chemotaxis and M13 phage infection kinetics (**Figure 2a**). The model simulation provided a comprehensive picture about the formation dynamics of V-shape infected zone (**Figure 1a**). The

infected cells produced new phages that would further infect more uninfected cells along the front of the migrating population at the same propagating speed as the host front migration speed. At the same time, the phages infected other neighboring bacteria, causing the lateral expansion of the infected region with an expanding speed. The bi-directional propagation results in a V-shaped infection region (the coral region in **Figure 1a**). Both the co-propagation front speed and lateral expansion speed were positively dependent on the host motility (**Extended Data Figure 4**), while the ratio of the two speeds determined the V-shaped angle θ, which defined how fast the viral spread during the co-propagation with host bacteria migration.

The dependence of viral spread on the host motility during co-propagation

We then examined experimentally how the V-shaped angle θ depended on the host bacterial motility by varying the agar concentrations. At high agar concentration, the probability of bacterial cells being trapped by the agar gel matrix increased, thereby reducing the bacterial motility[35,36]. For chemotactic bacterial population, which could enhance their group migration by following their self-generated chemoattractant gradient (known as navigated range expansion[12]), the speed of range expansion decreased as the agar concentration increased[37]. Interestingly, even though host bacterial motility was limited, the V-shaped infected zone increased given a fixed distance away from where the initial infection occurred (**Figure 1b**). We then quantified the V-shaped angle θ, which further showed a negative dependence on co-propagation speed (**Figure 1c**). Moreover, we observed that the negative relation

did not hold during the host unguided range expansion (**Extended Data Figure 5**). We also verified that this relationship did not depend on the geometric effect of radial expansion (**Extended Data Figure 6**). By varying the host effective diffusion coefficient, our model can reproduce the negative relation between host migration speed and viral spread during navigated range expansion (**Extended Data Figure 6b**). These evidences suggested a counterintuitive finding that the increase in host group migration speed would limit the phage spread during host navigated range expansion.

The model suggests that the co-propagation group migration speed also depended on the host chemotactic coefficient, which measures how responsive bacterial cells are to the environmental chemoattractant gradient[38]. The simulation results showed that the co-propagating speed of the host and phage increased linearly with the host chemotactic coefficient (**Extended Data Figure 7a**), much faster than the lateral expansion speed (**Extended Data Figure 7b&c**). As a result, the V-shaped angle θ, as well as the size of the phage-infected zone, decreased significantly when the host chemotactic migration speed increased (**Figure 2b&2c**).

We further tested the model prediction by measuring the V-shaped angle θ with a chemotactic coefficient titratable strain (ZF1). Specifically, we deleted the native regulation of a chemoreceptor gene *tar* in the bacterial genome, and introduced a titratable control of *tar* expression by a small molecule inducer, anhydrotetracycline (aTc) (See Methods, **Figure 3a**). The *tar* variant strain affected the receptor gain of

the cells in response to aspartate[21], but not the tumble bias or growth rate[39]. Therefore, by titrating different inducer aTc concentrations, we could manipulate the bacterial chemotactic migration speed (**Figure 3b, Extended Data Figure 8a**), but not the effective diffusion coefficients[38,39]. Under different host migration speeds, we measured the infected V-shaped angle θ and found it decreased as the migration speed increased (**Figure 3b, Extended Data Figure 8b&8c**). The experimental results confirmed our model prediction that virus spread is hindered by the host chemotactic migration.

The migratory culling of phages during co-propagation

Another important prediction of our model is that co-propagation of host bacteria and phage is not always sustained during the host navigated range expansion. As we decreased the phage production rate in the model, it resulted in a slower lateral expansion of the infected zone, limiting the V-shaped angle θ and the viral spread. At very low phage production rate, the V-shaped angle θ of the phage-infected zone became small. If we further increased the group migration speed, the size of the infected zone shrank until a sudden drop to almost zero, where infection only occurred near the initial spot of phage (**Extended Data Figure 10**). This indicated that the co-propagation of host bacteria and phage could not be maintained and the infected cells as well as the phages were culled from the propagating front. In other words, the system underwent a phase transition from co-propagation to migratory culling (**Figure 2b**).

To experimentally test the phase transition of migratory culling, we engineered both the M13 phage and its bacterial host to enable the titration of the phage production rate after infection. Specifically, we first deleted the *gIII* gene from the M13 phage genome and replaced by a T7 *rnap* gene (M13SP). The native GIII protein is essential for the M13 phage into a host bacterium, and deletion of GIII protein prevents full escape from the infected host[40,41]. In other words, the variant phage M13SP cannot be produced by wild type infected cells, as it lacks of *gIII* gene[42,43]. We then incorporated the *gIII* gene into bacterial host cells under a T7 promotor (strain FTT7, see method). When the M13SP infects the engineered host FTT7, the cells express the T7 RNAP whose gene is brought by the phage, which then activates the expression of GIII protein and restores the complete production of M13SP phage. Therefore, the variant phage M13SP infects the engineered strain FTT7 and generates a V-shaped infection zone during the co-propagation range expansion, and the dependence of V-shaped angle θ on the host migration speed is similar to the wild-type system (**Figure 3B**, **Figure4B**).

An important advantage of this engineered phage-bacteria system is that we can generate a series of engineered strains with T7 promotor variants that have different T7 RNAP binding affinities[40]. Here, we used a library of T7 promotor variants that we had previously characterized in our study[40]. The weak T7 RNAP binding affinity, e.g. FTG8 strain, reduces the GIII protein expression[44], resulting in a smaller V-shaped

zone (**Figure 4b**). Increasing the host migration speed further would lead to a much smaller V-shaped infected zone. However, for variant strains such as FTF10 and FTD8, whose protomer expression activity is much smaller than that of wild type T7 promoter, the V-shaped infected zone only exists at the slow host migration speed. When the host migration speed becomes large, the infected zone is confined to a small spot (**Figure 4b**). Away from the initial drop of phage, we verified that no infected bacteria or phage particles were carried, suggesting they were culled from the front propagation. We then systematically measured the angle of the V-shaped infected zone for a series of variant strains at different host migration speeds (**Figure 4d**). The phase transition from co-propagation to migratory culling is clearly observed at low promotor expression activity and fast host migration speed (**Figure 4d**), demonstrating the occurrence of migratory culling.

The spatial sorting mechanism of migratory culling

To understand the underlying mechanism of migratory culling, we then examined the simulated dynamics of the co-propagation front. The simulation results showed that the phage profile generally followed that of the infected cells. Although most of the cells were already infected in the middle of the co-propagation front, at the edge infected zone the uninfected cells and infected cells together formed a leading propagating front of bacterial host (**Figure 4e**). This propagating front is an important property for navigated range expansion, as it's generally a balance between local cell growth and back diffusion[12]. In the presence of phage infection, the increase of

infected cells also resulted from continuous conversion from uninfected to infected cells. Therefore, to cull the infected cell from the propagation front, it required the net growth of infected cells to be smaller than their back diffusion.

We then examined the detailed profiles of the uninfected and infected cells in the leading propagating front at the edge of the infected zone. The model revealed a spatial sorting structure of the uninfected and infected cells: the uninfected cells were located at the leading edge of the propagation front while the infected cells were located at the rear end (middle panel of **Figure 4e**). We also observed this spatial difference between uninfected and infected cells experimentally (right panel of **Figure 4e**). The spatial sorting structure of the two subpopulations in the propagation front indicated that the back diffusion of the infected cells was larger than that of the uninfected cells. Without the conversion from uninfected cells by phage infection, the infected cells could not keep up with the uninfected migration front. In the presence of moderate phage infection (e.g. low phage production by infected cells), the increase in migration speed leads to stronger total back diffusion[12,19], but the major increment came from the increase in the back diffusion of infected cells. Increasing the migration speed further or reducing the phage infection would make the back diffusion larger than the sum of self-growth of infected cells and conversion rate from uninfected cells, causing the infected cells to be culled from the migration front. This resulted in a transition from co-propagation to migratory culling of infected bacterial host and phage.

Discussion

The understanding of the interplay of host migration and viral spread has been developed with the advent of global change and advances in genetics, but the direct experimental tools are still lack[11,25,30]. Here, we developed a synthetic host-viral copropagating system to investigate how host motility affected viral spread during host navigated range expansion. We found a counterintuitive phenomenon that faster host chemotaxis-driven range expansion inhibited viral range expansion and resulted in a phase transition from co-propagation to migratory culling of phage.

Although migratory culling has been increasingly recognized in natural migratory animals and its role in regulating viral transmission dynamics, there is still a lack of agreement on how often and how much it may occur[45,46]. It is thought to depend on the extent to which infection affects the host's physiological and behavioral traits[47]. Our finding revealed that the temporary growth reduction during infection led to the spatial sorting of uninfected and infected host in the navigated propagation front, which resulted in a faster back diffusion of infected host that enabled their elimination. This quantitative understanding does not require complex infection-induced changes to host migrations, which has potential implications for controlling the spread of infectious diseases by altering the host motility or the virus production rate.

Long-term co-propagation would further lead to the co-evolution of host and virus

during range expansion, which could have consequences for the genetic diversity and adaptation of both host and virus populations[7,8]. In addition, our previous study utilized the bacteria-phage co-propagating system to develop a spatial phage-assisted continuous evolution system, which revealed the evolutionary process during co-propagation was accelerated compared to a fixed niche[40]. Therefore, the inhibition of viral spread by host migration discovered in this study would further help to improve the directed evolution method and provide new insights into host-viral co-evolution dynamics.

1. Xu, H., Dauparas, J., Das, D., Lauga, E. & Wu, Y. Self-organization of swimmers drives long-range fluid transport in bacterial colonies. *Nat Commun* **10**, 1792 (2019).
2. Mattingly, H. H., Kamino, K., Machta, B. B. & Emonet, T. Escherichia coli chemotaxis is information limited. *Nat. Phys.* **17**, 1426–1431 (2021).
3. Cao, Y., Neu, J., Blanchard, A. E., Lu, T. & You, L. Repulsive expansion dynamics in colony growth and gene expression. *PLoS Comput Biol* **17**, e1008168 (2021).
4. Hallatschek, O. & Nelson, D. R. Life at the front of an expanding population. *Evolution* **64**, 193–206 (2010).
5. Wu, Y., Kaiser, A. D., Jiang, Y. & Alber, M. S. Periodic reversal of direction allows Myxobacteria to swarm. *Proc. Natl. Acad. Sci. U.S.A.* **106**, 1222–1227 (2009).
6. Limdi, A., Pérez-Escudero, A., Li, A. & Gore, J. Asymmetric migration decreases stability but increases resilience in a heterogeneous metapopulation. *Nat Commun* **9**, 2969 (2018).
7. Ping, D. *et al.* Hitchhiking, collapse, and contingency in phage infections of migrating bacterial populations. *The ISME Journal* **14**, 2007–2018 (2020).
8. Heilmann, S., Sneppen, K. & Krishna, S. Coexistence of phage and bacteria on the boundary of self-organized refuges. *Proc. Natl. Acad. Sci. U.S.A.* **109**, 12828–12833 (2012).
9. Li, X., Gonzalez, F., Esteves, N., Scharf, B. E. & Chen, J. Formation of phage lysis patterns and implications on co-propagation of phages and motile host bacteria. *PLoS Comput Biol* **16**, e1007236 (2020).
10. Viboud, C. *et al.* Synchrony, Waves, and Spatial Hierarchies in the Spread of Influenza. *Science* **312**, 447–451 (2006).
11. Altizer, S., Bartel, R. & Han, B. A. Animal Migration and Infectious Disease Risk. *Science* **331**,

296–302 (2011).

12.Cremer, J. *et al.* Chemotaxis as a navigation strategy to boost range expansion. *Nature* **575**, 658–663 (2019).

13.Liu, W., Tokuyasu, T. A., Fu, X. & Liu, C. The spatial organization of microbial communities during range expansion. *Current Opinion in Microbiology* **63**, 109–116 (2021).

14.Wu, Y. & Berg, H. C. Water reservoir maintained by cell growth fuels the spreading of a bacterial swarm. *Proc. Natl. Acad. Sci. U.S.A.* **109**, 4128–4133 (2012).

15.Skellam, J. G. Random dispersal in theoretical populations. *Biometrika* **38**, 196 (1951).

16.Fisher, R. A. The wave of advance of advantageous genes. *Annals of Eugenics* **7**, 355–369 (1937).

17.Andow, D. A., Kareiva, P. M., Levin, S. A. & Okubo, A. Spread of invading organisms. *Landscape Ecol* **4**, 177–188 (1990).

18.Frankel, N. W. *et al.* Adaptability of non-genetic diversity in bacterial chemotaxis. *eLife* **3**, e03526 (2014).

19.Narla, A. V., Cremer, J. & Hwa, T. A traveling-wave solution for bacterial chemotaxis with growth. *Proc. Natl. Acad. Sci. U.S.A.* **118**, e2105138118 (2021).

20.Liu, W., Cremer, J., Li, D., Hwa, T. & Liu, C. An evolutionarily stable strategy to colonize spatially extended habitats. *Nature* **575**, 664–668 (2019).

21.Yu, D., Ma, X., Tu, Y. & Lai, L. Both piston-like and rotational motions are present in bacterial chemoreceptor signaling. *Sci Rep* **5**, 8640 (2015).

22.Bi, S. *et al.* Discovery of novel chemoeffectors and rational design of *Escherichia coli* chemoreceptor specificity. *Proc. Natl. Acad. Sci. U.S.A.* **110**, 16814–16819 (2013).

23. Krauss, S. *et al.* Coincident ruddy turnstone migration and horseshoe crab spawning creates an ecological 'hot spot' for influenza viruses. *Proc. R. Soc. B.* **277**, 3373–3379 (2010).

24. Waldenström, J., Bensch, S., Kiboi, S., Hasselquist, D. & Ottosson, U. Cross species infection of blood parasites between resident and migratory songbirds in Africa. *Molecular Ecology* **11**, 1545–1554 (2002).

25. Figuerola, J. & Green, A. J. Haematozoan Parasites and Migratory Behaviour in Waterfowl. *Evolutionary Ecology* **14**, 143–153 (2000).

26. Fritzsche McKay, A. & Hoye, B. J. Are Migratory Animals Superspreaders of Infection?: An Introduction to the Symposium. *Integr. Comp. Biol.* **56**, 260–267 (2016).

27. Altizer, S., Hobson, K. A., Davis, A. K., De Roode, J. C. & Wassenaar, L. I. Do Healthy Monarchs Migrate Farther? Tracking Natal Origins of Parasitized vs. Uninfected Monarch Butterflies Overwintering in Mexico. *PLoS ONE* **10**, e0141371 (2015).

28. Hall, R. J., Altizer, S. & Bartel, R. A. Greater migratory propensity in hosts lowers pathogen transmission and impacts. *Journal of Animal Ecology* **83**, 1068–1077 (2014).

29. Satterfield, D. A., Maerz, J. C. & Altizer, S. Loss of migratory behaviour increases infection risk for a butterfly host. *Proc. R. Soc. B.* **282**, 20141734 (2015).

30. Bartel, R. A., Oberhauser, K. S., De Roode, J. C. & Altizer, S. M. Monarch butterfly migration and parasite transmission in eastern North America. *Ecology* **92**, 342–351 (2011).

31. Folstad, I., Nilssen, A. C., Halvorsen, O. & Andersen, J. Parasite avoidance: the cause of post-calving migrations in Rangifer? *Can. J. Zool.* **69**, 2423–2429 (1991).

32. Krkošek, M. *et al.* Effects of host migration, diversity and aquaculture on sea lice threats to Pacific salmon populations. *Proc. R. Soc. B.* **274**, 3141–3149 (2007).

33. Shaw, A. K. & Binning, S. A. Migratory Recovery from Infection as a Selective Pressure for the Evolution of Migration. *The American Naturalist* **187**, 491–501 (2016).

34. Mysterud, A., Qviller, L., Meisingset, E. L. & Viljugrein, H. Parasite load and seasonal migration in red deer. *Oecologia* **180**, 401–407 (2016).

35. Licata, N. A., Mohari, B., Fuqua, C. & Setayeshgar, S. Diffusion of Bacterial Cells in Porous Media. *Biophysical Journal* **110**, 247–257 (2016).

36. Bhattacharjee, T. & Datta, S. S. Bacterial hopping and trapping in porous media. *Nat Commun* **10**, 2075 (2019).

37. Croze, O. A., Ferguson, G. P., Cates, M. E. & Poon, W. C. K. Migration of Chemotactic Bacteria in Soft Agar: Role of Gel Concentration. *Biophysical Journal* **101**, 525–534 (2011).

38. Fu, X. *et al.* Spatial self-organization resolves conflicts between individuality and collective migration. *Nat Commun* **9**, 2177 (2018).

39. Bai, Y. *et al.* Spatial modulation of individual behaviors enables an ordered structure of diverse phenotypes during bacterial group migration. *eLife* **10**, e67316 (2021).

40. Wei, T. *et al.* Exploiting spatial dimensions to enable parallelized continuous directed evolution. *Molecular Systems Biology* **18**, e10934 (2022).

41. Esvelt, K. M., Carlson, J. C. & Liu, D. R. A system for the continuous directed evolution of biomolecules. *Nature* **472**, 499–503 (2011).

42. Ploss, M. & Kuhn, A. Kinetics of filamentous phage assembly. *Phys. Biol.* (2010).

43. Smeal, S. W., Schmitt, M. A., Pereira, R. R., Prasad, A. & Fisk, J. D. Simulation of the M13 life cycle I: Assembly of a genetically-structured deterministic chemical kinetic simulation. *Virology* **500**, 259–274 (2017).

44. Thuronyi, B. W. *et al.* Continuous evolution of base editors with expanded target compatibility and improved activity. *Nat Biotechnol* **37**, 1070–1079 (2019).

45. Risely, A., Klaassen, M. & Hoye, B. J. Migratory animals feel the cost of getting sick: A meta□analysis across species. *Journal of Animal Ecology* **87**, 301–314 (2018).

46. Fritzsche McKay, A. & Hoye, B. J. Are Migratory Animals Superspreaders of Infection?: An Introduction to the Symposium. *Integr. Comp. Biol.* **56**, 260–267 (2016).

47. Bradley, C. A. & Altizer, S. Parasites hinder monarch butterfly flight: implications for disease spread in migratory hosts. *Ecology Letters* **8**, 290–300 (2005).

48. Neidhardt, F. C., Bloch, P. L. & Smith, D. F. Culture Medium for Enterobacteria. *J Bacteriol* **119**, 736–747 (1974).

49. Leonard, S. P. *et al.* Genetic Engineering of Bee Gut Microbiome Bacteria with a Toolkit for Modular Assembly of Broad-Host-Range Plasmids. *ACS Synth. Biol.* **7**, 1279–1290 (2018).

50. Baer, A. & Kehn-Hall, K. Viral Concentration Determination Through Plaque Assays: Using Traditional and Novel Overlay Systems. *JoVE* 52065 (2014) doi:10.3791/52065.

51. Liu, C. *et al.* Sequential Establishment of Stripe Patterns in an Expanding Cell Population. *Science* **334**, 238–241 (2011).

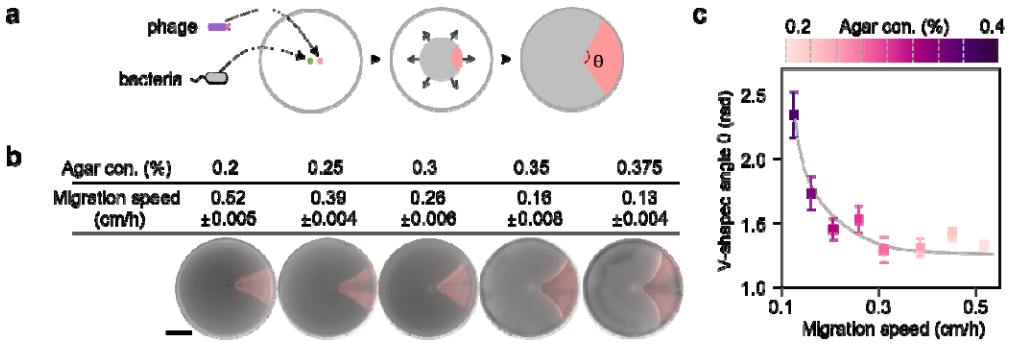

Figure 1 The phage spread during the bacterial navigated range expansion.

a, The co-propagation of bacteria and phage leads to a V-shaped infected zone. **b**, The typical migration speeds and V-shaped infected zone (light pink zone) under different agar concentrations. E.coli FM15 was inoculated at the center of a semisolid agar plate (D-RMD medium + 100uM aspartate) with different agar concentrations, and the reporter phage M13-ruby3 was inoculated 1 cm away from the center. The infected cells expressed red fluorescent protein *ruby3* which was introduced by phage during infection. The merged pseudo-color image is a combination of brightfield and fluorescence images. **c**, The dependence of V-shaped θ angle on the bacteria migration speeds by varying agar concentrations. Strain detail is given in **Supplementary Table 1**. Scale bar, 2 cm. Data were taken 96 h after inoculation.

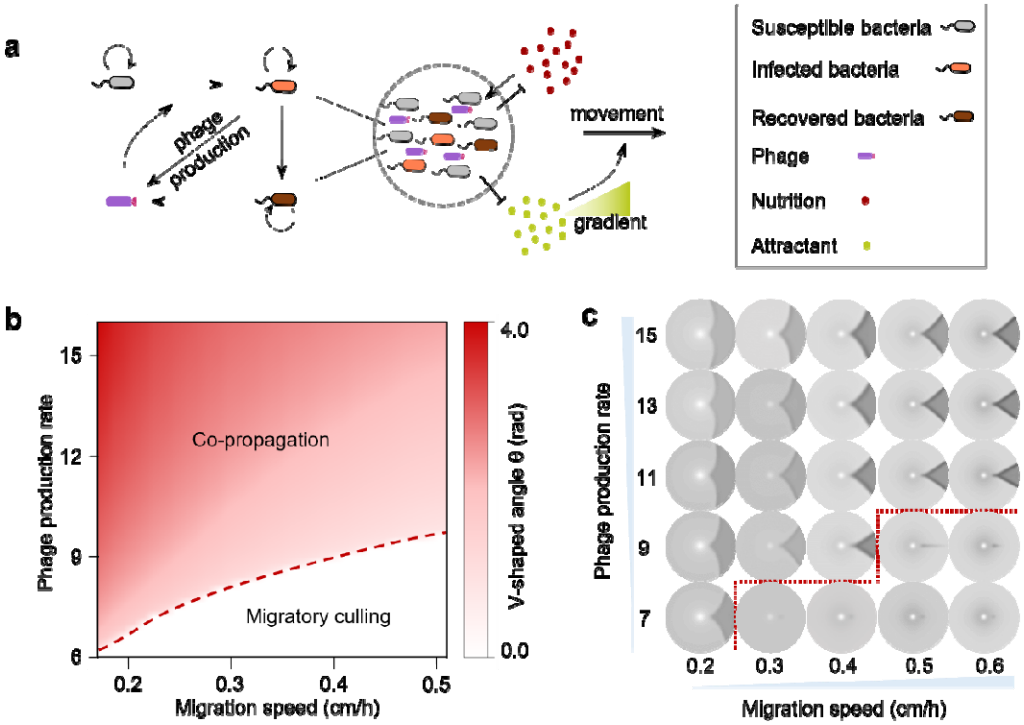

Figure 2 Kinetic model of the interaction between bacteria and phage.

a, Schematic illustration of population's navigated range expansion. Bacterial populations navigate forward unoccupied territories that depend on the chemo-attractants gradients. The bacterial populations are classified into three categories: susceptible, infected, and recovered bacteria. Infected bacteria are converted from susceptible bacteria by phage infection, and eventually become recovered bacteria. These three bacterial populations all proliferate by consuming the nutrition. Motile bacteria expand their range into unoccupied territories by diffusion and chemotaxis. In the meantime, the nonmotile phages are transmitted by their host bacteria, and their titer depends on the level of infectious progeny phage production rate by infected and recovered bacteria. **b**, Simulated phase diagram of bacterial-viral co-propagation. The model predicted that the angle of phage spread was negatively correlated with the bacteria migration speed by varying the chemotactic coefficient (the same as varying diffusion coefficient, see **Supplementary Figure 3**) and positively correlated with the phage production rate. The system experienced a phase transition from co-propagation to migratory culling as further increasing migration speed at low phage production rates (red dashed line). **c**, The typical V-shaped patterns under the different migration speeds and phage production rates.

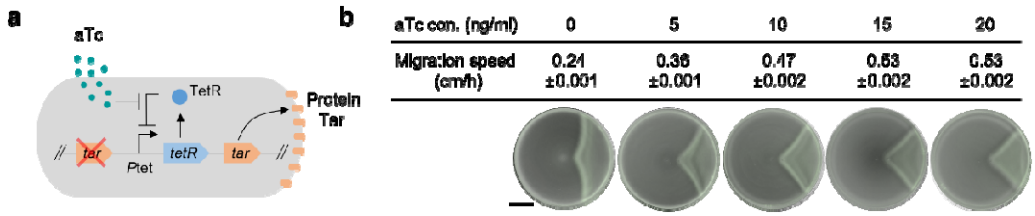

Figure 3 The phage spread under different co-propagating migration speeds by titration of host bacteria chemotactic abilities

a, Design of the chemotactic ability titratable strain ZF1 by inducible expression of chemotactic receptor protein Tar. **b**, The typical migration speeds and V-shaped patterns under different anhydrotetracycline (aTc) concentrations. Scale bar, 2 cm. Data were taken 30 h after inoculation.

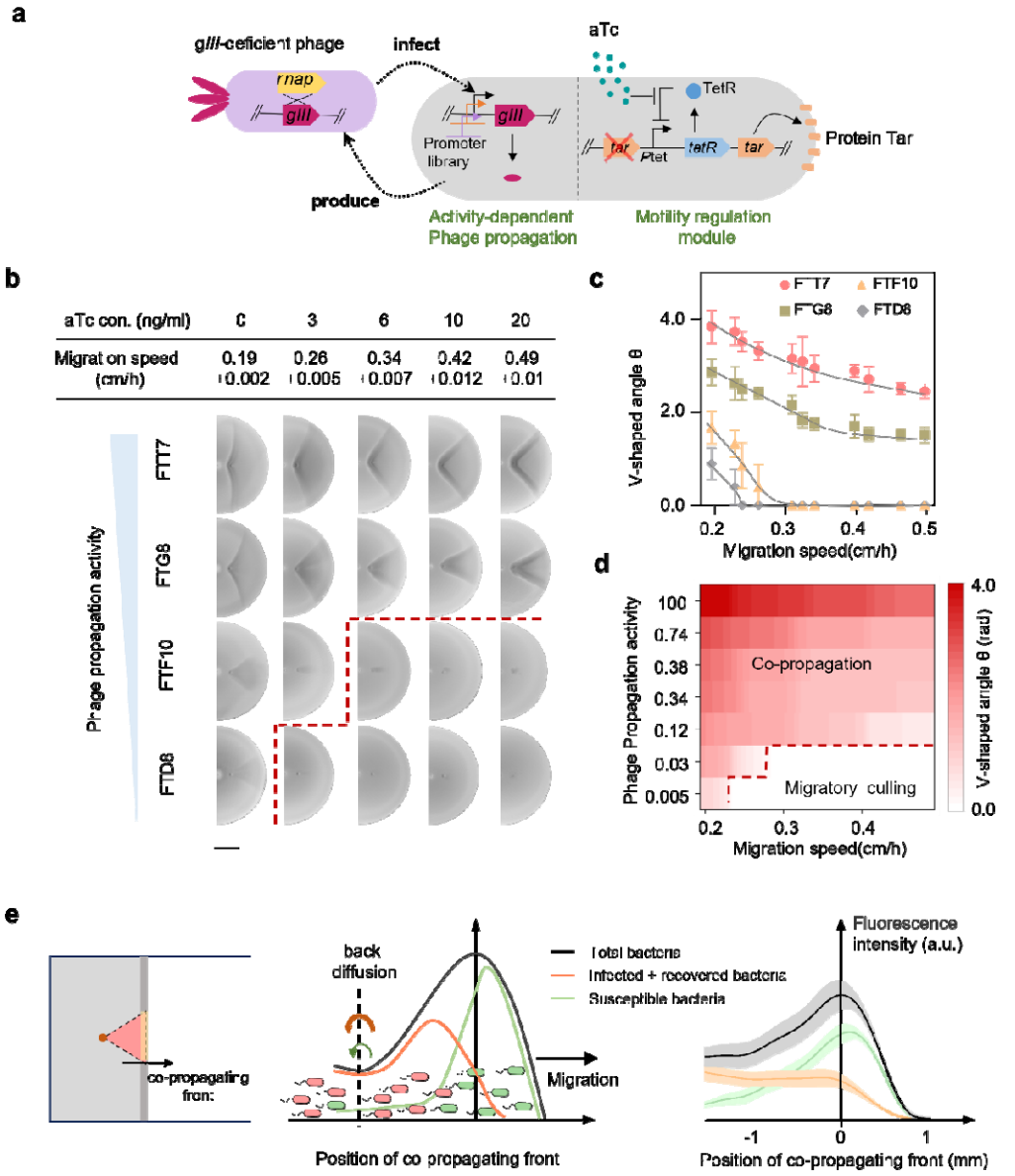

Figure 4. The phase transition and the spatial sorting mechanism of migratory culling. a, Schematic design of the chemotactic titratable strain ZF1 coupling T7 RNAP activity with the expression of *gIII*. The host bacteria carry a motility regulation module and an activity-dependent phage propagation module, which are harbored by chromosome and the accessory plasmid, respectively. **b**, The typical migration speeds and V-shaped patterns for the typical strains (FTT7, FTG8, FTF10, and FTD8) under different anhydrotetracycline (aTc) concentrations. **c**, The detailed relationship between the angle of the fan□shaped pattern and the migration speed in **b**. **d,** The phase transition of migratory culling by seven strains with different phage propagation activities (The detailed sequences of T7 promoter variants were shown in **Supplementary Table S2**) under different aTc concentrations. The angle of phage spread was negatively correlated with the bacteria migration speed and positively correlated with the phage production rate, and the migratory culling happened under the higher migration speed and lower phage production rate. **e**, The spatial sorting mechanism of migratory culling. Along the co-propagating front near the edge between infected and uninfected zone (as the

arrow in the left panel), the simulated density profiles (middle panel) showed a spatial sorting structure of infected + recovered cells (orange line) and the susceptible cells (green line), which further led to a smaller back diffusion for the susceptible cell (green arrow) than that of infected + recovered cells (orange arrow). The co-propagation profiles (the right panel) of ZF1-Ruby (a plasmid carrying red fluorescent gene *ruby* was inserted into the strain ZF1, **Supplementary Table S1**) and phage M13-GFP (a *gfp* gene was integrated into phage genome) demonstrated the spatial sorting structure experimentally. The profiles of total (black) and infected + recovered bacteria (green) were directly quantified the red and green fluorescent signals respectively, while the profile of susceptible bacteria (orange) was calculated by the other two profiles. The colored shallow was the error bar of the profiles from three independent experimental replicates.

Method

Media and growth conditions

The Luria-Bertani (LB) medium contained 10g tryptone, 5g yeast extract, and 5g NaCl per liter. The defective rich defined medium (D-RDM) used in this study was based on the Neidhardt's lab recipe[48] and modified: 1× MOPS mixture, 0.25 × ACGU, 1× defective amino acid mixture (a mixture of 17 amino acid excluding asparagine, aspartic acid and serine, named as 1×AA), 1.32 mM K_2HPO_4, 100μM aspartic acid(K salt, 0uM only for the host unguided range expansion experiment) and 0.4% (w/v) glucose. Mops salts and ACGU were prepared to be 10 X MOPS and 10X ACGU stocks solution. The defective amino acid mixture 1×AA was prepared to be 5×AA stocks solution (in 1l): 356.36mg alanine, 5478.2mg arginine (HCL), 87.83mg cysteine (HCL), 611.49mg glutamic acid (K salt), 438.6mg glutamine, 300.28mg glycine, 209.6mg histidine (HCL H_2O), 262.4mg isoleucine, 524.8mg leucine, 365.4mg lysine, 149.2mg methionine, 330.4mg phenylalanine, 230.2mg proline, 238.2mg threonine, 102.1mg tryptophane, 181.2mg tyrosine, 351.6mg valine. All the medium in this study was buffered to pH 7.0 with 0.1M HEPES (pH 7.0).

To prepare semi-solid plates, the bacto-agar (BD,214010) was added to the growth medium, and the agar concentration varied from 0.2% to 0.4%(w/v). If required, inducer anhydrotetracycline (aTc) was also added to the medium and its concentration varied from 0 to 20 ng/ml. Then, 10 ml of the above medium supplemented was poured into a 90-mm Petri dish and allowed to harden at room temperature for 60 min in a light-proof box. In addition, the medium was supplemented with chloramphenicol (25 μg/ml), spectinomycin (50 μg/mL), tetracycline (10 μg/mL), kanamycin (10 μg/mL) and ampicillin (20 μg/mL). All experiments were executed at 37°C unless otherwise specified.

The culture condition of Figure 1 and Extended Data Figure 6 (FM15 with different agar concentrations): D-RMD medium + 100uM aspartate + 0.2%~0.4% agar concentration + 10 μg/mL tetracycline;

The culture condition of Extended Data Figure 5 (Ft-MGΔcheRcheB with different agar concentrations): D-RMD medium + 0.2%~0.4% agar concentration + 10 μg/mL tetracycline;

The culture condition of Figure 3 and Extended Data Figure 8 (ZF1 with different aTc concentrations): D-RMD medium + 100 uM aspartate +0 ~ 20 ng/ml aTc + 0.2% agar concentration + 10 μg/mL kanamycin + 20 μg/mL ampicillin;

The culture condition of Figure 4b&4c&4d (Strains of the FT series, FTT7/FTA1/FTD5/FTD8/FTD9/FTF10/FTG8: the chemotactic titratable strain ZF1 coupling T7 RNAP activity with the expression of gIII): D-RMD medium + 100 uM aspartate +0 ~ 20 ng/ml aTc + 0.25% agar concentration+ 10 μg/mL kanamycin + 50 μg/mL spectinomycin;

The culture condition of Figure 4e (ZF1-Ruby): D-RMD medium + 100 uM aspartate + 20 ng/ml aTc + 0.25% agar concentration + 10 μg/mL kanamycin;

Strains and phages construction

The strains and plasmids used in this study are listed in Supplementary Table S1. The Escherichia coli CLM strain was provided by Dr Chenli liu[20] and all other strains in this study, except *E. coli* K12 strain ER2738, were derived from it. The strain FM15 was a conjugation of the *E. coli* CLM and the *E. coli* K12 ER2738 (NEB, F plasmid with tetracycline-resistant provider) and was provided by Dr Chenli Li[40]. Based on the understanding of the molecular mechanism about chemotactic signal transduction of E.coli, we constructed a chemotactic defect E.coli strain Ft-MG△cheRcheB by the following steps: (i) we constructed a chemotactic defect E.coli MG△cheRcheB by knocking the chemotactic gene cheR and cheB of E.coli CLM; (ii) we transferred the psim5 plasmid with chloramphenicol gene into the strain MG△cheRcheB and obtained the strain MG△cheRcheB-psim5 (cultured in 30°C); (iii) we conjugated the

recipient strain MG△cheRcheB-psim5 with the donor strain FM15 (F plasmid provider) and got a strain Ft-MG△cheRcheB-psim5; (iv) removed the psim5 plasmid by culturing in 37°C and obtained the strain Ft-MG△cheRcheB. The tar-titratable strain MGT was constructed as follows: (i) the strain CLM(Δtar) was obtained by knocking the chemotactic receptor protein Tar gene of the strain CLM. (ii) the bla:Ptet-tetR-tar feedback loop was amplified and inserted into the strain CLM(Δtar) chromosomal attB site utilizing λRed homologous recombination, then we obtained the strain MGT. The strain FkP was constructed by replacing the tetA-PtetA/tetR-tetR cassette of F plasmid in the strain Er2738 with the kanamycin-resistance gene. The tar-titratable strain ZF1 was a conjugation of the strain MGT and the strain Fkp (F plasmid with Kan resistant provider). The strain FTT7 was constructed by electroporating the plasmid AP-T7 (T7 RNAP-dependent accessory plasmid contain M13 phage gene III with a wild type T7 promoter, gift from Dr Chenli Liu[40]) into the strain ZF1, and the similar strain FTA1/FTD5/FTD8/FTD9/FTF10/FTG8 was constructed by electroporating the plasmid AP-A1/ AP-D5/ AP-D8/ AP-D9/ AP-F10/ AP-G8 (The variants of plasmid AP-T7 with T7 promoter variants, and the details of the promoter sequence was shown in Appendix Table S1, gifts from Dr Chenli Liu[40]) into the strain ZF1. To better capture the location difference of the infected and uninfected cells in the co-propagating front, we constructed the strain ZF1-Ruby, in which a red fluorescence plasmid PZA31-Ptet-M2-mRuby with chloramphenicol gene was inserted into the strain ZF1.

The phage M13 used in this study was a gift from Dr Chenli Liu[40] and others were its variants. To better characterize the infectious state of the bacteria, the coding sequence of green/red fluorescence protein gene was inserted into the genome of M13 and the strain was designated as M13-GFP, M13-RFP and M13-Ruby. The phage SP-YFP was also provided by Dr Chenli Liu[40], in which *gene III* of the M13 genome was deleted and replaced by a T7 RNP with a downstream yellow fluorescence protein gene. All phages were verified by sequencing.

Conjugation of F plasmid

The conjugation of F plasmid is based on the Barrick laboratory's recipe[49], and the detailed protocol is as follow: (i) grow overnight cultures of donor and recipient strains in the presence of diaminopimelic acid (DAP, 0.3 mM) and appropriate antibiotic. (ii) gently spin down 1 mL culture (~6000 rpm for 3 minutes) and wash donor and recipient cells in PBS, then repeat and resuspend in 500 µL PBS. (iii) measure cell density and combine 1:1 ratio of donor and recipient cells in micro centrifuge tube (100 µL:100 µL). (iv) plate 200 µL of mixture onto non-selective LB medium plate containing DAP, and then incubate conjugation plate overnight. (v) scrape up the conjugation mixture into a micro centrifuge tube with 1 mL PBS, vortex and gently spin down and repeat, then resuspend conjugation mixture in 1 mL of PBS and plate 100 µL of this mixture and 100 µL of a 10-fold dilution onto selective plates. (vi) pick single colonies and culture in selective media and confirm the strain via PCR amplification of the target strains.

Growth curve measurement

The growth curves of uninfected and infected bacteria were measured in a 250-ml flask with 50ml corresponding growth medium at 37°C, 150rpm. The general procedure was as follows. First, the isolated bacteria from −80 °C stock was streaked onto the agar plate with LB medium and cultured at 37 °C overnight. Second, 3-5 single colonies were picked and inoculated into 14ml round-bottom test tubes containing 2ml LB medium and cultured overnight in a shaker (220 rpm, Shanghai Zhichu Instrument) as the seed-culture procedure. Third, the overnight seed-cultures were diluted into 2ml D-RDM medium by a ratio of 1:100 and grown to log-phase the next morning; when the diluted cultures reached OD_{600} 0.2~0.3, the diluting step was repeated. Fourth, 5ml the cultures (OD_{600} around 0.2-0.3) were added into a 250-ml flask with 45ml prewarmed D-RDM medium and were cultured in a water-bath shaker (150 rpm, Shanghai Zhichu Instrument). When the diluted cultures reached an

OD_{600} of 0.2, 2ml bacteria culture was added to 48 ml prewarmed D-RDM medium with or without phage (10^9 pfu M13-GFP was pre-added in the experiment of infected cells and 0 pfu in that of uninfected cells). The medium was then incubated and measured. The samples were taken every 10 min for measurement of OD_{600} by using spectrophotometer reader until bacterial cells entered the stationary phase. For phage growth assay, one-milliliter samples were extracted at the same time points and filtered through a 0.22μm pore size PES syringe filter to remove bacterium. Aliquots for the time series were then stored at -20°C until tittering. The growth curve was illustrated in Appendix Fig S1.

Phage propagation and tittering

The strain FM15 was served as host bacteria for propagating and tittering M13 phage. Cells used for phage propagation were cultured in 20ml LB medium until they reached OD600= 0.3-0.4 and then infected with 10^9 pfu of phage. The bacteria-phage mixture was incubated overnight at 37°C. Cell debris was removed by centrifugation at 5000 rpm for 10min and filtration. The fresh supernatant containing the revived phage were collected and stored at -20°C for up to several months. To determinate the phage titer, we employed the double agar overlay plaque assay as described in previous work[50]. Bottom agar for plates and soft agar for overlayers were LB broth containing 1.5% and 0.4% Bacto agar, respectively. Serial ten-fold dilutions of the phage stock and the underlay agar plates were prepared in advance. We transferred 10μl of the selected dilution of phages to a tube of 3 ml warm overlay medium, immediately added 100μl culture of the host bacterium (OD600 around 0.3-0.4), mixed and poured the contents over the surface of a dried and labeled underlay plate. The overlays were allowed to harden for 30 min and then incubated at 37°C overnight. The following day, we counted plaques on plates with 30–300 plaques and defeminated the titer of the original phage stock by using the following calculation: Number of plaques×100×reciprocal of counted dilution = pfu ml^{-1}.

Expansion experiment procedures

First, the isolated bacteria from −80 °C stock was streaked onto the agar plate with LB medium and cultured at 37 °C overnight. 3-5 single colonies were picked and inoculated into 14ml round-bottom test tubes containing 2ml LB medium and cultured overnight in a shaker (220 r.p.m., Shanghai Zhichu Instrument) as the seed-culture procedure. Second, the overnight seed-cultures were diluted into 2ml D-RDM medium by a ratio of 1:100 and grown to log-phase the next morning, and then were further diluted in the same way when the diluted cultures reached OD_{600} 0.2~0.3. In the experiment of measuring host's range expansion speed, bacteria were then cultured to the mid-log phase (OD_{600} was around 0.2–0.3), which was inoculated at the line 2cm away from the center of a semi-solid agar plate using a 75-mm glass slide for the plane-wave range expansion. Alternatively, 2 μl of the strain was inoculated at the center of a semi-solid agar plate for the normal range expansion. In the virus infection experiment procedures, 2μl M13 phages with different concentrations were inoculated 1 cm away from the bacteria position, and then incubated at 37 °C for several hours until the bacteria occupied the whole plate. For the experiment of measuring bacteria expansion speed, only bacteria strain was inoculated and incubated at 37 °C.

Bacteria expansion speed measurement

The semi-solid agar plate was illuminated from below by a circular white LED array with a light box as described previously[51] and imaged at 1 h or 2 h intervals using a Canon EOS 600D digital camera. Images were analyzed using ImageJ. For the normal range expansion, a circle was fitted to the intensity maximum in each image and the area (Ar) of the fitted circle was determined. The radius (r) of the colony was calculated as $r = \sqrt{Ar/\pi}$. The maximum expansion speed was calculated using a linear fit over a sliding window of at least five time points, with the requirement that the fit has an R^2 greater than 0.99. For the plane-wave range expansion, an image analysis script using MATLAB was written to find the front peak position of the images at different time and then we got the mean migration speed by a linear fitting.

Angle of V-shape pattern calculation

When the semi-solid agar plate was occupied by bacteria, brightfield images of the plates were captured by the image device in above Method and fluorescence images were captured using the UVP CHEMSTUDIO™ TOUCH 815 IMAGERS (Analytik Jena, US). Virus spread intensity can be represented by the angle of the fan-shape pattern and can be determined as follows. Using ImageJ analysis to fluorescence images, the phage infection area (*A*) of the fixed region (*L* centimeter away from the initial phage inoculation position) was calculated, and the angle of the fan-shape pattern was $\theta = 2A/L^2$.

Fluorescence intensity assay

To investigate the location difference of the infected and uninfected cells in the propagating front (Box. D), the plates were scanned by Nikon Ti-E microscopy equipped with a 10× phase contrast objective (Nikon CFI Plan Fluor DL4X F, N.A. 0.13, W.D. 16.4 mm, PhL), the green and red fluorescence was taken with a 2-ms and 500-ms exposure time, respectively. The details were as follows: firstly, as the above-mentioned method, the semi-solid D-RDM medium plate with 0.25% agar and 20 ng/ml aTc was prepared (see Media and growth conditions), and the strain ZF1-Ruby was cultured; Second, the strain ZF1-Ruby was inoculated at the line 2cm away from the center of the plate and 2μl 10^9 pfu/ml M13-GFP phage was inoculated 1 cm away from the bacteria position, and the plate was incubated at 37 °C for 10 hours; Third, the Fluorescence intensity of the whole propagating front in the plate was scanned by the Nikon Ti-E microscopy and the data was exported by the NIS-Elements AR software (ver. 4.50.00). The red fluorescence intensity represents the host cell ZF1-Ruby including the uninfected and infected cells, and the green fluorescence intensity represent the infected cells which express the green fluorescence gene of M13-GFP because of the phage infection. Hence, the uninfected cell can be represented by the red fluorescence intensity minus the green fluorescence

intensity. This was processed using a custom-written MATLAB code.

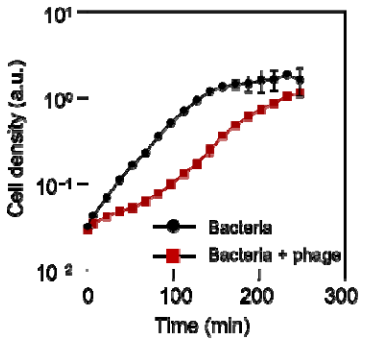

Extended Data Figure 1 Growth curves of E. coli FM15 before and after infection.

E. coli FM15 cells were cultured in LB broth. Bacteria are FM15 cells without phage inoculation; Bacteria + phage are cells with 10^9 PFU/ml of M13 phages added at time point 0.

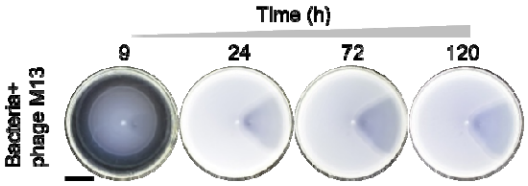

Extended Data Figure 2 Time-lapse photographs of typical patterns obtained for bacteria FM15 with phage M13. The scale bar represents 2 cm.

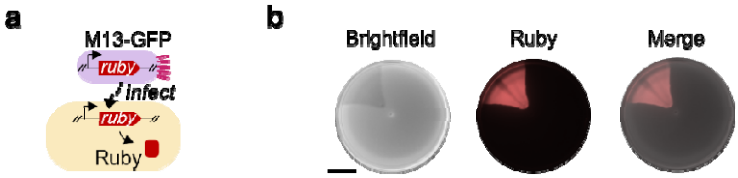

Extended Data Figure 3 Formation of the fan□shaped pattern by phage infection during bacterial range expansion. (**a**) Design of a reporter phage M13□ruby for fluorescence imaging of phage□infected region. (**b**) Visualization of infected region. Escherichia coli FM15 was inoculated at the center of a semisolid agar plate and the reporter phage M13□ruby was inoculated 1 cm away from the center. Fluorescence images (Materials and Methods) were captured after overnight incubation. The scale bar represents 2 cm.

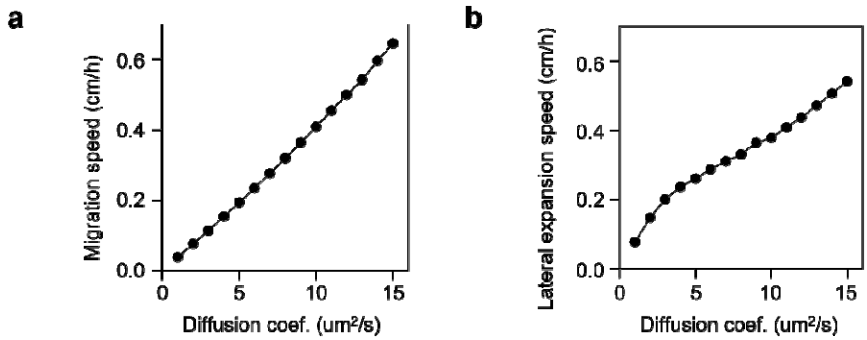

Extended Data Figure 4 The simulation of the diffusion coefficient's effect on speed. (a) The relationship between the host motility and co-propagation front speed. (**b**) The relationship between the host motility and lateral expansion speed.

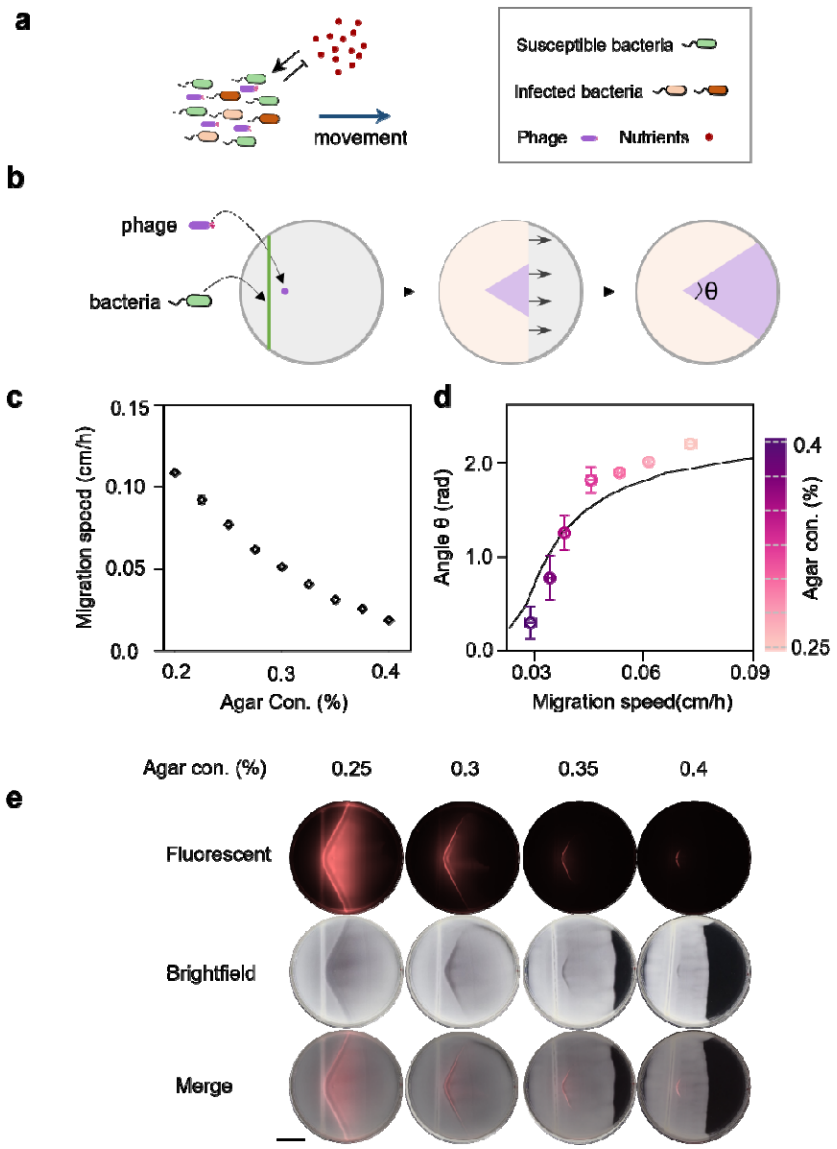

Extended Data Figure 5 The phage spread among the bacteria Ft-ΔcheRcheB under the plane wave with unguided range expansion. (**a**) Schematic illustration of the population's unguided range expansion. (**b**) Phage propagation during bacterial range expansion under the plane wave leads to the formation of a visible fan□shaped region of lower cell density. (**c**) The relationship between the agar concentration and the migration speed. (**d**) The experiment (circles) and simulation (line) show that the angle of the fan□shaped pattern is positively correlated with the bacteria migration speed. (**e**) The typical V-shaped patterns under different agar concentrations. Defective Escherichia coli Ft-ΔcheRcheB was inoculated at the line of a semisolid agar plate and the reporter phage M13-ruby3 was inoculated 1 cm away from the center. The scale bar represents 2 cm

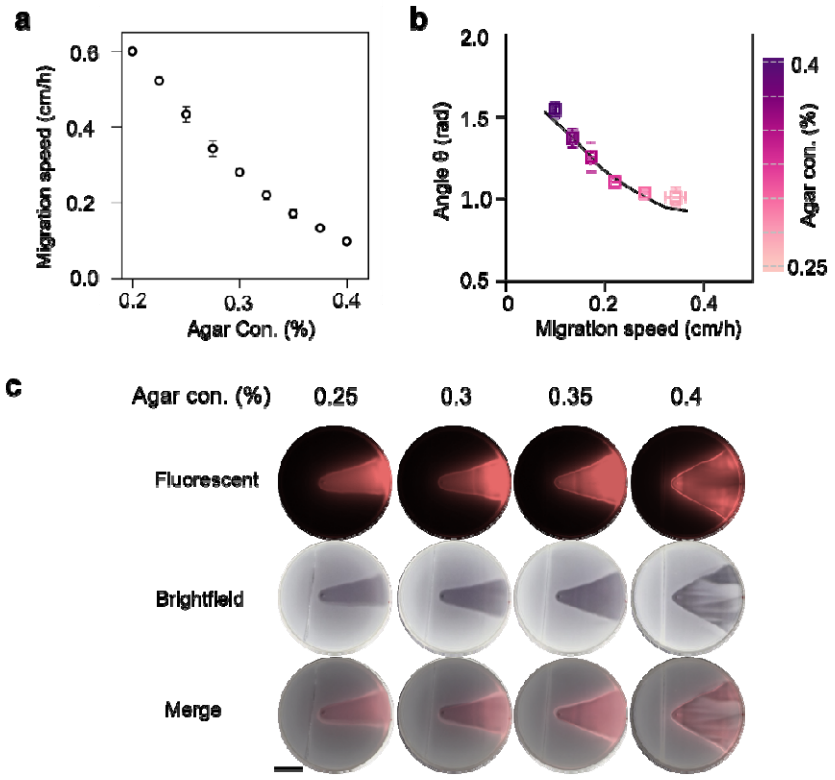

Extended Data Figure 6 The phage spread among the bacteria FM15 under the plane wave with navigated range expansion. (**a**) The relationship between the agar concentration and the migration speed. (**b**) The experiment (squares) and simulation (line) show that the angle of the fan□shaped pattern is negatively correlated with the bacteria migration speed. (**c**) The typical V-shaped patterns under different agar concentrations. Escherichia coli FM15 was inoculated at the line of a semisolid agar plate and the reporter phage M13□ruby3 was inoculated 1 cm away from the center. The scale bar represents 2 cm.

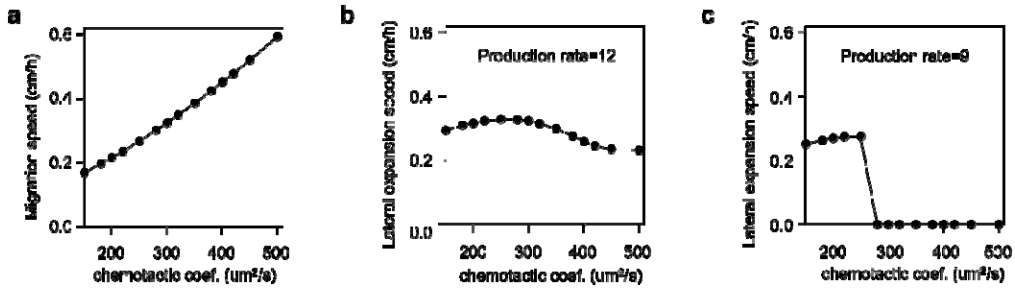

Extended Data Figure 7 The simulation of the chemotactic coefficient's effect on speed. (**a**) The relationship between host chemotactic coefficient and the co-propagation front speed. (**b**) The relationship between host chemotactic coefficient and lateral expansion speed for the higher production rate PR=12. (**c**) The relationship between host chemotactic coefficient and lateral expansion speed for the lower production rate PR=9.

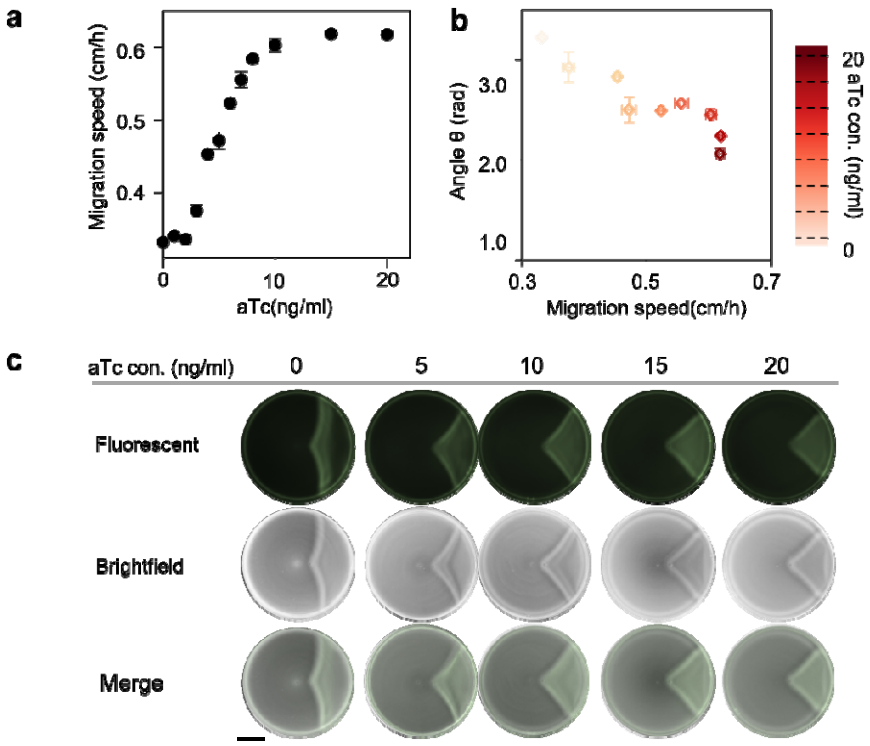

Extended Data Figure 8 The phage spread among the bacteria ZF1 regulated by different aTc concentrations. (**a**) Relationship between the aTc concentration and the migration speed. (**b**) The experiment shows that the angle of the fan□shaped pattern is negatively correlated with the bacteria migration speed. (**c**) The typical V-shaped patterns under different aTc concentrations. Escherichia coli ZF1 was inoculated at the center of a semisolid agar plate and the reporter phage M13□GFP was inoculated 1 cm away from the center. The scale bar represents 2 cm.

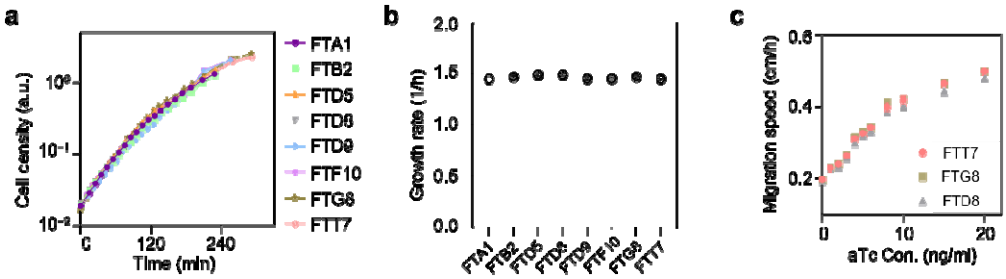

Extended Data Figure 9 The phenotypic characteristics for the strains with different T7 RNAP activities. (**a**) The growth curve for the eight strains with different T7 RNAP activities. (**b**) The growth rate for the eight strains with different T7 RNAP activities. (**c**) The relationship between the aTc concentration and the migration speed for the strain FTT7, FTG8 and FTD8.

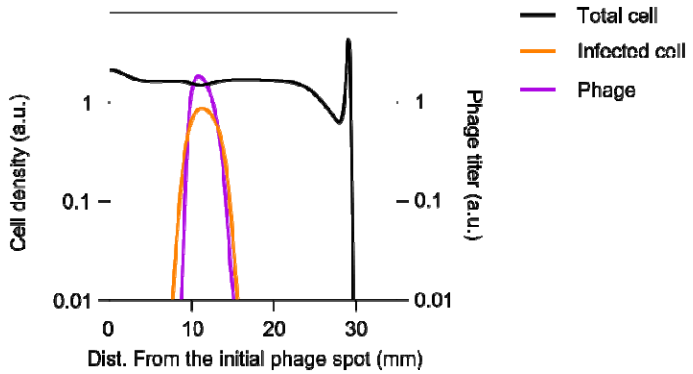

Extended Data Figure 10 Profiles of the cell intensity and phage titer along the central radial line of the fan□shaped infection zone in the simulation result for χ=440 and α=7.

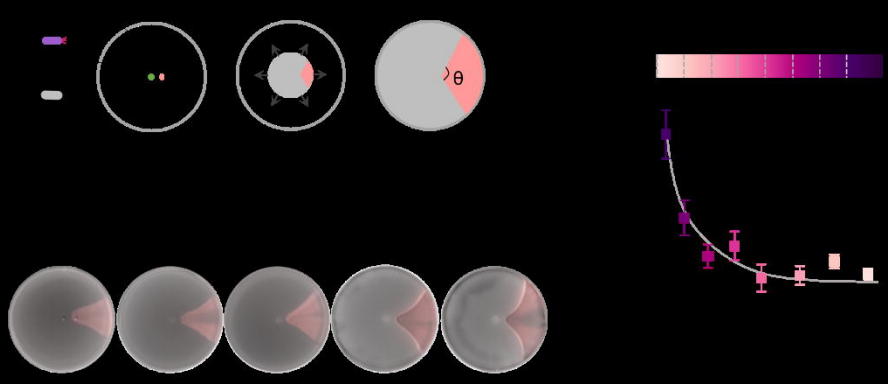
θ

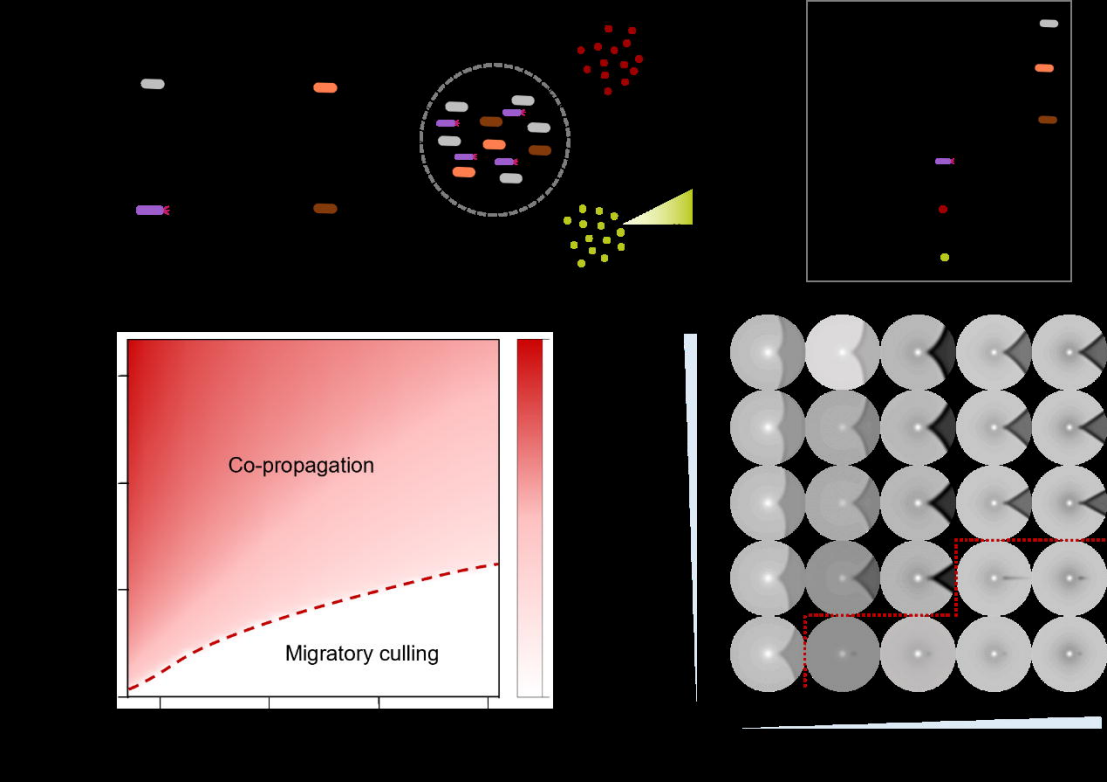
Co-propagation
Migratory culling

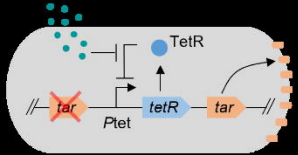
TetR
tar
Ptet
tetR
tar

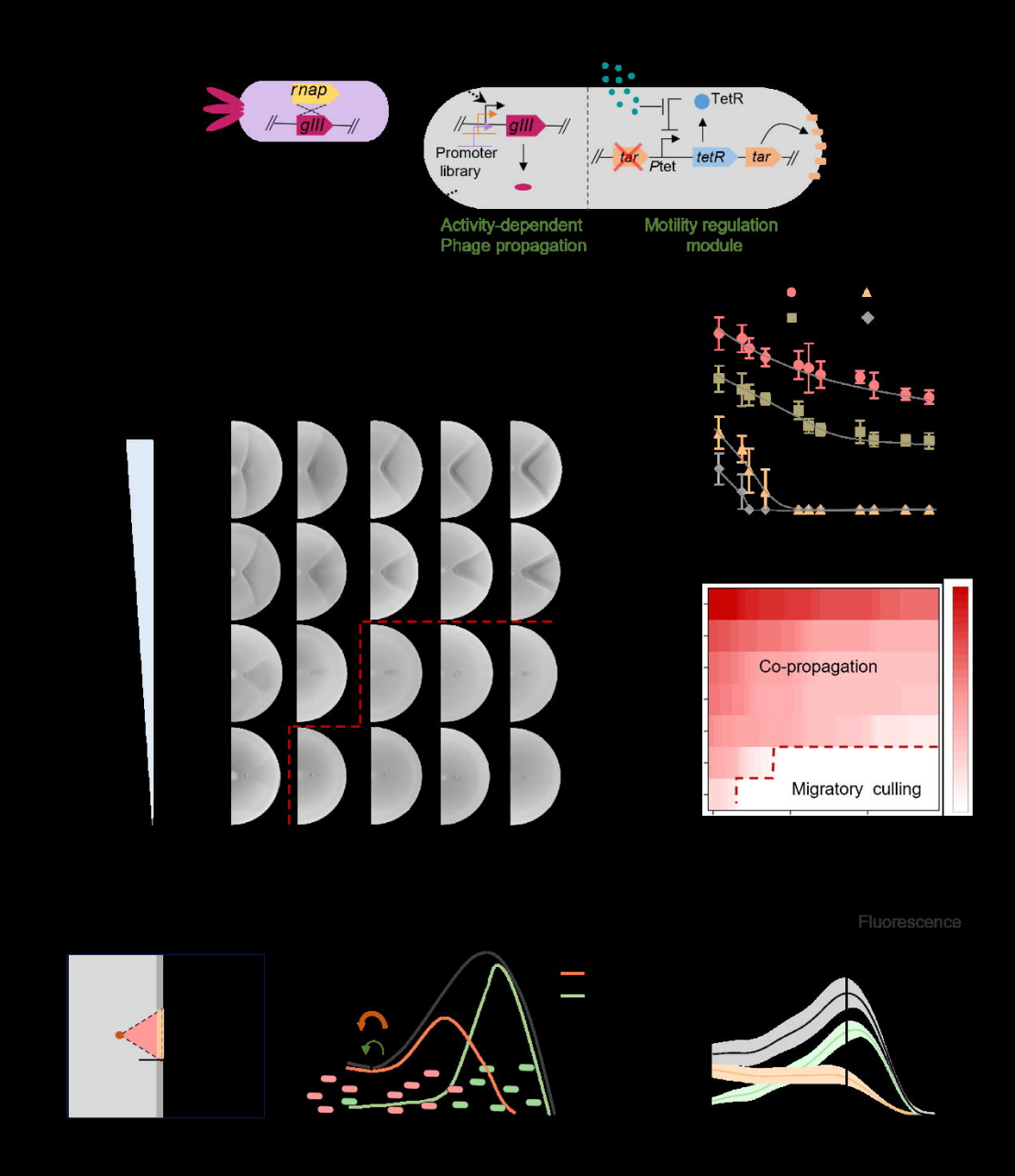
rnap
gIII
gIII
Promoter library
TetR
tar
Ptet
tetR
tar
Activity-dependent Phage propagation
Motility regulation module
Co-propagation
Migratory culling
Fluorescence

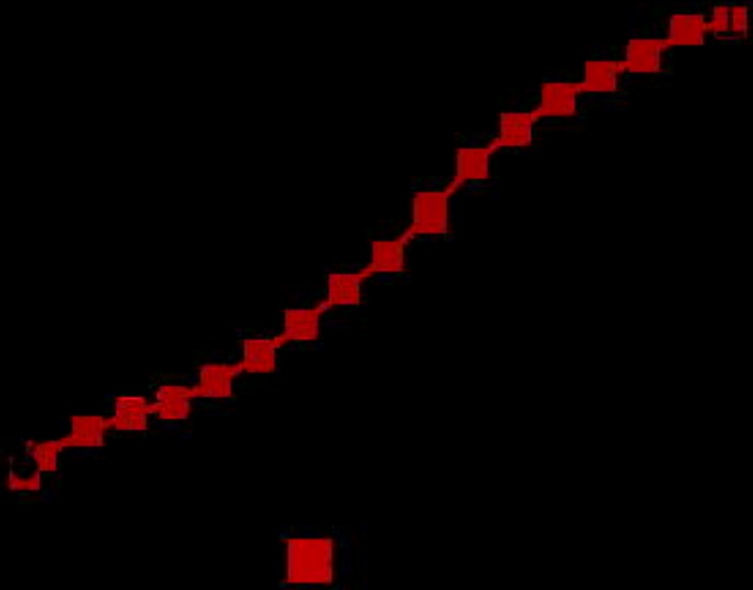

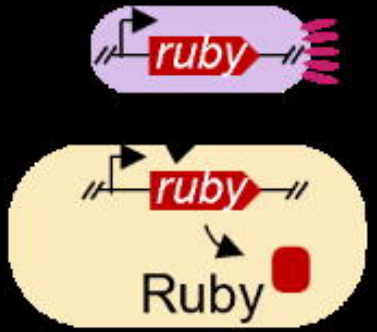
ruby
ruby
Ruby

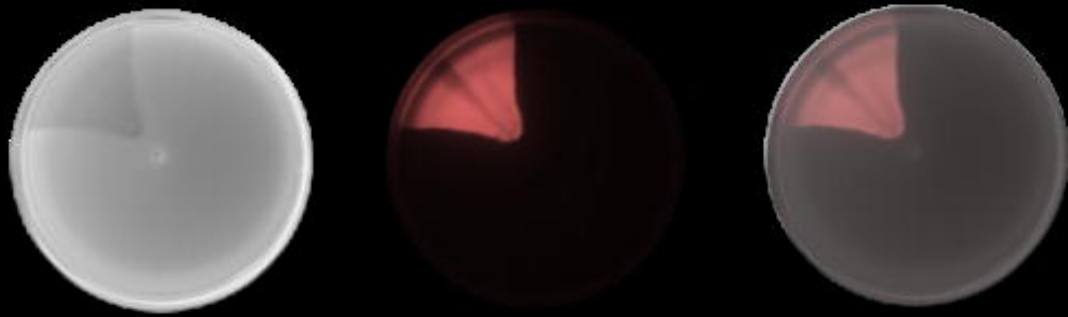

θ

0.2
0.3
0.4

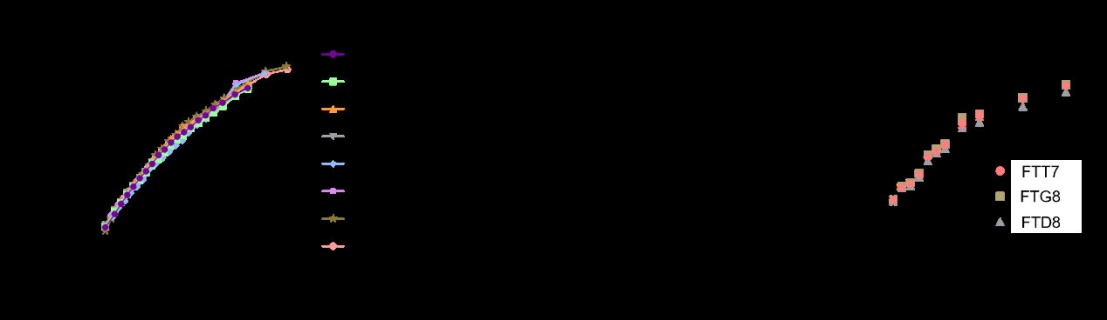
FTT7
FTG8
FTD8